In-Vivo Measurement of Dynamic Joint Motion Using High Speed Biplane Radiography and CT: Application to Canine ACL Deficiency

Scott Tashman[1]

William Anderst

Bone and Joint Center,
Henry Ford Hospital,
2799 W. Grand Blvd.,
Detroit, MI 48202

Dynamic assessment of three-dimensional (3D) skeletal kinematics is essential for understanding normal joint function as well as the effects of injury or disease. This paper presents a novel technique for measuring in-vivo skeletal kinematics that combines data collected from high-speed biplane radiography and static computed tomography (CT). The goals of the present study were to demonstrate that highly precise measurements can be obtained during dynamic movement studies employing high frame-rate biplane videoradiography, to develop a method for expressing joint kinematics in an anatomically relevant coordinate system and to demonstrate the application of this technique by calculating canine tibio-femoral kinematics during dynamic motion. The method consists of four components: the generation and acquisition of high frame rate biplane radiographs, identification and 3D tracking of implanted bone markers, CT-based coordinate system determination, and kinematic analysis routines for determining joint motion in anatomically based coordinates. Results from dynamic tracking of markers inserted in a phantom object showed the system bias was insignificant (−0.02 mm). The average precision in tracking implanted markers in-vivo was 0.064 mm for the distance between markers and 0.31° for the angles between markers. Across-trial standard deviations for tibio-femoral translations were similar for all three motion directions, averaging 0.14 mm (range 0.08 to 0.20 mm). Variability in tibio-femoral rotations was more dependent on rotation axis, with across-trial standard deviations averaging 1.71° for flexion/extension, 0.90° for internal/external rotation, and 0.40° for varus/valgus rotation. Advantages of this technique over traditional motion analysis methods include the elimination of skin motion artifacts, improved tracking precision and the ability to present results in a consistent anatomical reference frame. [DOI: 10.1115/1.1559896]

Keywords: Kinematics, Motion Analysis, Knee, Radiography, ACL

Introduction

Dynamic assessment of three-dimensional (3D) skeletal kinematics is essential for understanding normal joint function as well as the effects of injury or disease. Joint motion is driven by a combination of dynamic physical forces (gravitational, inertial and contact), active muscular forces and constraints imposed by passive structures (articular surface geometry, ligaments, etc.) [1,2]. The specific combinations of these forces occurring during most activities are unknown. Thus, natural joint behavior cannot be reproduced in cadaveric studies, and can only be revealed by *in-vivo* studies of typical movement activities.

Conventional motion measurement methods employ either optoelectronic or video-based systems to track markers attached to the skin. These systems are non-invasive, easy to use and work well for many clinical and research motion analysis applications. However, studies utilizing implanted bone pins have shown that markers affixed to the skin shift relative to underlying bone by as much as 30 mm, particularly during rapid movements or activities involving impact such as heelstrike [3–5]. This marker tracking error varies with bone, marker position, activity and joint angle and is often correlated with the movement, complicating efforts to develop algorithms for error correction [6]. Techniques have been developed combining large numbers of skin markers with algorithms to detect violations of the rigid body assumption and model soft tissue deformation [7–9]. *In-vivo* validation of these techniques has been limited, but one study of tibial tracking for a single subject performing a low-speed 10 cm step-up demonstrated substantially reduced errors in estimated bone motion (average error 0.8 mm, peak error approx. 2.6 mm) [10]. However, the authors acknowledge that the fixation pins that enabled direct bone tracking may have reduced skin movement. Additionally, errors would likely increase for the femur (due to greater soft tissue between markers and bone), and during more dynamic activities (e.g. gait, running, jumping) where skin deformation is greater and more difficult to model.

When fully validated, these advanced surface marker techniques may improve the accuracy of kinematic data from surface markers sufficiently to meet the needs for most clinical and research motion analysis studies. If the kinematic measurements are to be used in conjunction with musculoskeletal models to estimate dynamic loads and stresses on joint tissues, however, then even errors as small as 1 mm may be unacceptable. For example, when estimating strains in the anterior cruciate ligament (ACL), a ±1 mm error in tibio-femoral displacement could introduce an uncertainty in the ligament length of approximately ±3% (assuming a

[1]Corresponding Author: Scott Tashman, Ph.D., Head, Motion Analysis Section, Henry Ford Hospital, 2799 W. Grand Blvd., ER2015, Detroit, MI 48202 . Telephone: (313) 916-8680; FAX: (313) 916-8812; E-mail: tashman@bjc.hfh.edu

Contributed by the Bioengineering Division for publication in the JOURNAL OF BIOMECHANICAL ENGINEERING. Manuscript received October 2001; revised manuscript received October 2002. Associate Editor: M. L. Hull

nominal ligament length of 30 mm). This error is similar in magnitude to estimated peak ligament elongation occurring during common activities such as stair climbing [11]. For investigating cartilage deformation, this error magnitude would be even less acceptable. A 1 mm displacement would be equivalent to a cartilage strain of approximately 25%, relative to the average thickness of healthy tibio-femoral cartilage [12]. A displacement error of this magnitude would translate into huge differences in estimates of contact forces.

It is possible to avoid skin motion artifacts by directly measuring bone movement, either by physically attaching measurement devices to the bone or via medical imaging techniques. Accurate *in-vivo* kinematics studies have been performed using external marker arrays rigidly fixed to bone [13,14]. However, the risks and discomfort associated with this technique are likely to limit the number of willing volunteers, and may make serial studies impossible. Dynamic MRI and CT methods show promise [15,16], but are limited by low frame rates and environments too restrictive for most dynamic, weight-bearing activities. Conventional fluoroscopy permits direct visualization of bone motion, but is limited to two-dimensional assessment and is prone to errors due to parallax and motion blur.

Biplane or stereo radiographic imaging enables accurate quantitative 3D motion assessment as well as direct visualization of bone motion. Use of biplane radiographic film methods (Radiostereometric analysis or RSA) for 3D studies of static bone position has been well established [17,18], with precision reported in the $\pm 10-250$ μm range [19]. The goals of the present study were threefold as follows: 1) to demonstrate that similar precision can be obtained during dynamic movement studies by combining high frame-rate biplane video-radiography with analysis techniques similar to RSA, 2) to develop a method for expressing joint kinematics in an anatomically relevant coordinate system, and 3) to demonstrate the application of this technique by calculating canine tibio-femoral kinematics during dynamic motion.

Methods

Four components were used to implement the method: a hardware system for generation and acquisition of high frame rate biplane radiographs, a software package for identification and 3D tracking of bone markers, a CT-based system for coordinate system determination and a set of kinematic analysis routines for determining joint motion in anatomically based coordinates. The application of this method for studying canine ACL deficiency is described here, though the method has been applied similarly to human studies.

Radiographic Imaging System. The high-speed biplane radiography system consists of two 150 kVp X-ray generators (Shimadzu Medical Systems, model AI5765HVP) and two 30 cm image intensifiers (Shimadzu Medical Systems, model UD150B-10) optically coupled to synchronized high-speed video cameras (JC Labs HSC-250, $512\times240\times8$-bit pixels, 250 frames/s), configured in a custom gantry to enable a variety of motion studies (Fig. 1). This system was set up in a configuration commonly used for gait testing (60° inter-beam angle, X-ray source to object distance 1.3 m, and object to intensifier distance 0.5 m). Images were acquired with the generators in continuous radiographic mode (100 mA, 90 kVp). The video cameras were electronically shuttered (1/2000 s) to reduce motion blur. To minimize radiation exposure, short (0.5-1 s) sequences were recorded, with X-ray exposure and image acquisition controlled by an electronic timer/sequencer and synchronized to the desired phase of movement (using accelerometers and/or optical sensors). Raw (uncompressed) video data were captured with two 40 MHz frame grabbers (Epix 4MIP Model 12), and saved to computer disk for subsequent analysis.

Radiopaque Bone Markers. As with static RSA, implanted radiopaque bone markers were employed to enable accurate registration between the two views. A minimum of three markers per bone was necessary for 3D analysis; more markers could have improved accuracy but also increased the likelihood of marker overlap. As in conventional RSA, tantalum spheres were selected because of their biocompatibility and high radio-density, though somewhat larger markers (1.6 mm diameter, vs. 0.8 mm typical for film-based RSA) were needed to compensate for the inherently poorer resolution and contrast of video-radiographs as compared to radiographic film. Markers were implanted in the distal femur and proximal tibia (percutaneously with a cannulated drill), with the goals of maximizing inter-marker spacing (in terms of distances and included angles to avoid co-linearity) and avoiding marker overlap in the radiographic views. No effort was made to locate markers at specific anatomical locations.

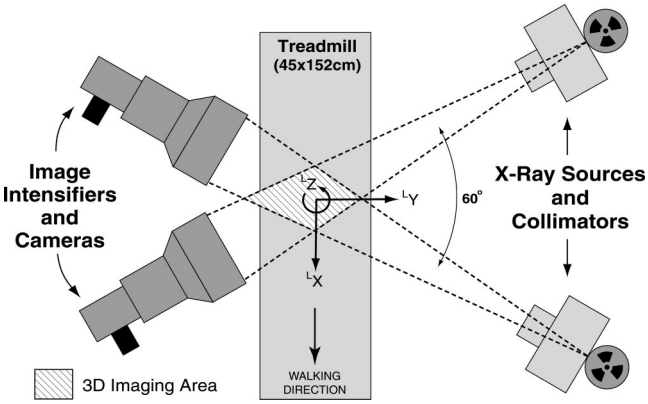

Fig. 1 An overhead diagram of the biplane radiographic imaging system, configured for treadmill testing. 3D imaging can occur in the area where the two X-ray beams intersect.

3D Marker Tracking. The radiographic process introduces significant defects in the acquired images that must be corrected to minimize 3D tracking errors. In particular, image intensifiers are known to introduce geometric distortion of 10% or more, and also suffer from non-uniform intensity response that can degrade image quality. These defects must be corrected prior to image processing and 3D tracking. Before each motion study, biplane images were acquired for bright and dark fields for intensity nonuniformity correction. Images were also acquired of a uniform 567-marker grid affixed to the face of each image intensifier (removed prior to dynamic imaging studies). These images were used to perform aspect ratio and distortion correction for all subsequent video frames, using a previously described method [20]. A pair of corrected images from a typical motion sequence is shown in Fig. 2.

Software was developed to search for marker signatures in each image frame, taking advantage of the known size and density distribution of the markers. Gray-scale weighted centroids were calculated for each marker with sub-pixel resolution. The resulting 2D coordinates were stored in a format compatible with commercial motion analysis software (EVa, Motion Analysis Corp.). This process was fully automated, and required approximately 6 seconds per frame on an SGI Octane (175 MHz processor).

Before and/or after the dynamic trials, biplane image sequences were obtained of a 10 cm acrylic cube containing twelve brass spheres (3 mm diameter) at known locations (within the milling machine tolerance of $+/-0.025$ mm). The EVa software was used to perform 3D camera calibration and coordinate reconstruction, using the calibration cube data and a modified Direct Linear Transformation method (DLT) [21]. EVa automatically matches marker trajectories from the two views, and provides graphical tools for confirming proper tracking. Final 3D marker locations for each motion frame were smoothed using a 4^{th} order, zero-lag

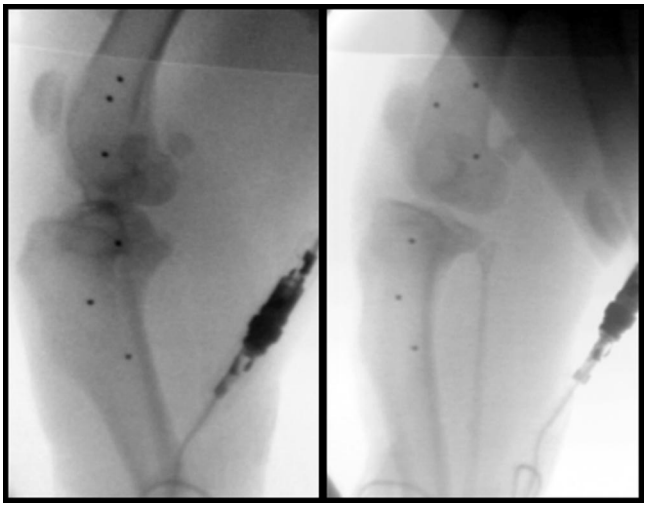

Fig. 2 Biplane radiographic images of a canine hindlimb, from a representative frame acquired during treadmill gait. The images have been corrected for nonuniformity and distortion, as described in the text. Three implanted tantalum markers can be clearly seen in each bone. The connector and wire for the skin mounted accelerometer (used to detect pawstrike) are also visible.

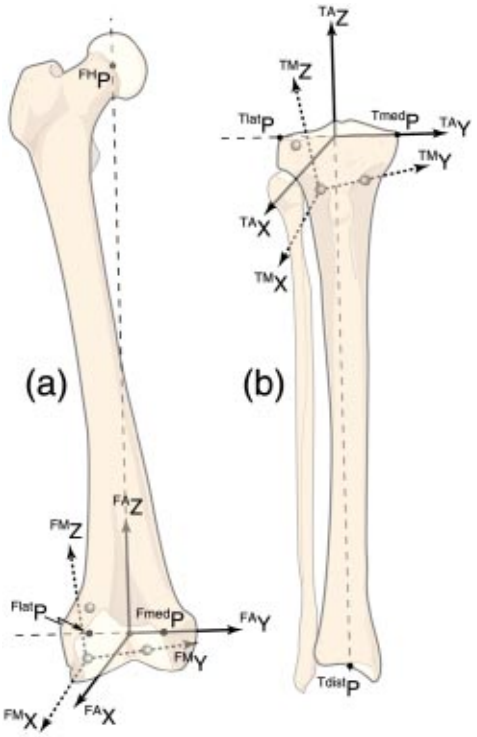

Fig. 3 Two local coordinate systems for the right femur (a) and tibia (b) are determined from the CT-generated 3D bone models. A marker-based orthogonal femur coordinate system (^{FM}X, ^{FM}Y, ^{FM}Z) is determined using cross products of the vectors defined by the implanted markers. An anatomically based orthogonal femur coordinate system (^{FA}X, ^{FA}Y, ^{FA}Z) is defined using the positions of the lateral and medial femoral condyles (^{Flat}P, ^{Fmed}P) and the center of the femoral head (^{FH}P). For the tibia, marker-based (^{TM}X, ^{TM}Y, ^{TM}Z) and anatomical (^{TA}X, ^{TA}Y, ^{TA}Z) coordinate systems are defined similarly, using the lateral and medial borders of the tibial plateau (^{Tlat}P, ^{Tmed}P) and the center of the distal tibia (^{Tdist}P).

Butterworth low-pass filter with a cutoff frequency of 25 Hz. This frequency was determined by residual analysis of several trials [22].

CT-Based Coordinate System Determination. Kinematic data must be expressed in an anatomically meaningful coordinate system for clinical relevance. 3D bone models, developed from computed tomography (CT), have been used previously to determine transformations between instrumentation-based and anatomically based coordinate systems [24]. A similar technique was employed to determine transformations between marker-based and anatomical coordinate systems, as shown in Fig. 3 and described below.

After radiopaque marker insertion, CT scans (transverse-plane, slice thickness 1 mm in regions containing markers, 5 mm in the rest of the bone, slice resolution 0.488 mm/pixel) were acquired for the tibia and femur. Locations of the tantalum markers within the bone volume were determined from the CT slices using the public domain NIH Image program (developed at the U.S. National Institutes of Health and available on the Internet at http://rsb.info.nih.gov/nih-image/). The location of the center of each marker signature was determined to the nearest 1/2-slice (0.5 mm with 1 mm slice spacing), and the nearest pixel within that slice. A local reference frame was constructed for each bone using three bone markers, describing the orientation of the marker-based coordinate systems relative to the CT-based coordinate system.

The stack of CT image slices was then reconstructed into a 3D bone model using Delaunay triangulation, as implemented in the Nuages software package [25]. The reconstructed 3D bone models were viewed on an SGI Octane computer using custom designed Open Inventor-based programs. Locations of anatomical landmarks for the femur (center of the lateral and medial condyles, and center of the femoral head) and the tibia (outermost edge of the lateral and medial condyles, and center of the distal end of the tibia) were interactively identified in the 3D bone models (Fig. 3). Once the anatomical markers were placed in the bone model, the locations of the anatomical markers with respect to the CT volume were known. The orientation of the anatomical coordinate systems relative to the marker-based coordinate systems could then be determined for the femur and tibia, using standard rigid-body transformations.

Calculating Joint Rotations. The three body-fixed rotation angles of the tibial anatomical coordinate system relative to the femoral anatomical coordinate system were calculated for each motion frame in the order flexion/extension, ab/adduction and internal/external rotation, applying the method described by Kane [26]. Using this convention, flexion/extension occurred about the femur anatomical y-axis (defined by the medial and lateral condyles), internal/external rotation occurred about the tibia anatomical z-axis (the long axis of the tibia), and ad/abduction occurred about a floating intermediate axis (mutually perpendicular to the other two axes). The resulting angles corresponded to the rotational component of the joint coordinate system described by Grood and Suntay [27].

Calculating Joint Translations. Joint translation is defined as the relative displacement between specific points fixed to each bone. No standard exists for the selection of these points on the tibia and femur. Since the primary application for this study was ACL injury and repair, the origin and insertion sites of the ACL were selected for displacement determination. Prior to postmortem CT scanning, additional radiopaque markers were fixed to the bone surfaces (with cyanoacrylate adhesive) at the approximate center of the ACL origin and insertion sites. The locations of the origin and insertion points were calculated from the CT slice data using the same process previously described for calculating

the locations of the tantalum markers in the femur and tibia. The vector from femoral origin to tibial insertion was defined and expressed in the tibial anatomical coordinate system. Thus, anterior/posterior (A/P) translation occurred along the tibia anatomical x-axis, medial/lateral (M/L) translation occurred along the tibia anatomical y-axis, and proximal/distal (P/D) translation occurred along the tibia anatomical z-axis. This coordinate system was selected for translations because it was both orthogonal and fixed to the tibia (with the A/P and M/L axes approximately parallel to the tibial plateau). Thus, the distance between ACL origin and insertion could be calculated as the magnitude of the vector defined by the three components of translation. With the ACL intact, this distance reflected the functional length of the ligament, assuming the ligament was not lax as is generally true for the canine knee [28]. In the ACL-deficient knee, it provided a single measure of the increased motion associated with ACL loss.

Experimental Validation. Accuracy is typically quantified in terms of bias and precision [29]. The conditions for performing accuracy tests should resemble actual testing conditions to the greatest extent possible to recreate imaging conditions, movement speeds, and other factors that could influence measurement accuracy. Therefore, precision and repeatability were estimated from *in-vivo* data. Bias was estimated from phantom tests however, because no alternative method was available for determining *in-vivo* inter-marker distances with high accuracy.

Measurement bias was assessed by tracking a moving acrylic phantom with two 1.6 mm diameter spherical targets placed 30 mm apart (using a milling machine with tolerance of approximately ± 0.025 mm). The object was suspended from a stiff elastic band and then dropped, allowing it to twist and bounce throughout the field of view. Biplane radiographic images of the motion were acquired at 250 frames/s, and 3D marker coordinates were determined. No smoothing or filtering was performed. Distance between the markers was calculated for 100 motion frames, and a t-test was performed to determine if the measured distance was significantly different from the 'true' value of 30 mm.

Precision and repeatability were assessed *in-vivo* using data from a biplane radiographic study of canine gait. This study was performed previously to investigate the effects of ACL loss on knee kinematics and joint degeneration. Three or more 1.6 mm tantalum spheres were implanted into the right tibia and femur of each dog. One month after marker implantation, tibial-femoral kinematics were assessed during treadmill gait with the ACL intact (ACL-I). The ACL was then surgically transected. After allowing 2 months for wound healing, the kinematic studies were repeated for the ACL-deficient condition (ACL-D). CT scans of the limbs were acquired (as described above) 24 months after ACL transection. The Henry Ford Health System Institutional Animal Care and Use Committee (IACUC) approved all animal procedures.

Kinematic data was collected at 250 frames/s using the biplane radiographic system described above. Three trials were collected for each test date (ACL-I and ACL-D) during treadmill walking at 1.5 m/s (Fig. 4). Elapsed time between ACL-I and ACL-D tests was 12 ± 2 weeks. Paw-strike timing was determined from a lightweight accelerometer strapped to the lower right hindlimb, and data was acquired from 0.2 s before to 0.3 s after paw-strike. Three-dimensional marker trajectories were calculated from the radiographic image data and low-pass filtered (25 Hz), as described above. Five dogs from this study were selected to investigate measurement system performance.

Repeatability and precision were assessed using inter-marker distance. It was assumed that the location of the implanted markers within the bone remained constant for the duration of the study. For each bone, a triangle was formed by selecting three implanted markers. For each frame of movement data, the lengths of the legs of the triangle as well as the angles included by the triangle were determined. Means and standard deviations of these measurements for each dog were calculated for the femur and tibia for both ACL-I and ACL-D tests.

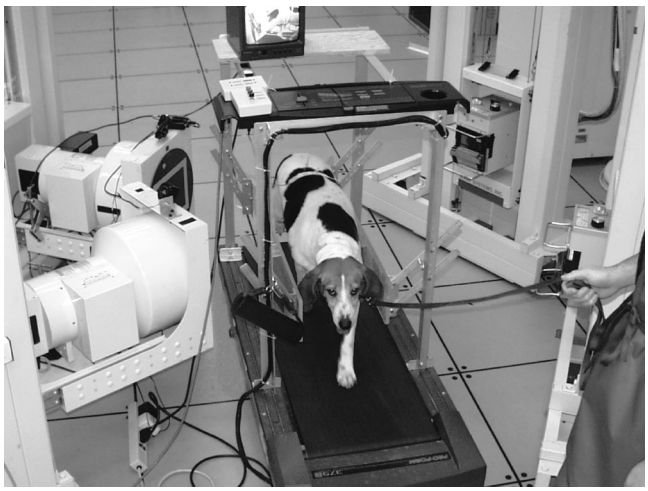

Fig. 4 A canine test in progress. Acrylic side-rails were used to maintain proper hindlimb positioning. Note the open nature of the system configuration, enabling a variety of movement tasks to be performed in the imaging space.

In-vivo precision was evaluated by examining the standard deviations of inter-marker distances and angles across all frames within a trial [29]. Since it was assumed that markers were rigidly fixed in bone for any selected trial, these distances/angles should be constant. Thus, frame-to-frame variations in these quantities provide a direct estimate of the three-dimensional precision of the measurement system. This analysis was performed with data from the ACL-I tests only.

Repeatability of anatomical marker placement was determined by interactively identifying the locations of the femur anatomical markers five times in each subject. Marker placement was performed by the same individual during multiple sessions spread over several days. The mean 3D location and standard deviation were calculated for each anatomical marker.

Repeatability of the tibio-femoral kinematic measurements was assessed by comparing multiple trials acquired during each test session. Dynamic joint rotations and displacements were calculated for three trials, and the resulting curves were synchronized in time by aligning the frames corresponding to paw-strike. Standard deviations were then determined at every frame for each kinematic variable across the three trials. No time normalization was performed, as it was assumed that stride times would be consistent from trial to trial within a test session (since walking speed was treadmill-controlled). A single repeatability measure for each set of three trials was determined by averaging the frame-by-frame standard deviations across the entire range of data valid in all three trials (typically, 60 or more frames).

Results

Dynamic tracking of markers inserted in the phantom object showed the mean inter-marker distance was 29.98 mm $+0.10$ mm. Compared to the 'true' distance of 30 mm, the system

Table 1 Measurement System Bias

	Distance (mm)
True	30
Mean	29.98
S.D.	0.10
Range	0.53

Table 2 Measurement System Precision

	Within-Trial Standard Deviations: Inter-Marker Distances (mm)		Within-Trial Standard Deviations: Inscribed Angles (deg)	
	(a) ACL-I	(b) ACL-D	(c) ACL-I	(d) ACL-D
dog 1	0.085	0.082	0.39	0.38
dog 2	0.065	0.092	0.25	0.37
dog 3	0.058	0.068	0.48	0.55
dog 4	0.053	0.050	0.21	0.19
dog 5	0.058	0.067	0.20	0.23
Average	**0.064 mm**	**0.072 mm**	**0.31°**	**0.35°**

bias was −0.02 mm (Table 1). This corresponded to a 0.07% error in distance, which was not significantly different from zero ($p > 0.05$).

In-vivo inter-marker spacing and relative orientation of implanted markers varied considerably from dog to dog. On the first test day (ACL-I), inter-marker distances averaged 18.33 ±5.5 mm (mean±standard deviation), with a range of 5.5 to 31.6 mm. Mean inter-marker distance was nearly identical for the second test session (ACL-D), at 18.32 mm. Included angles from the marker triads ranged from 16° to 122°.

For the ACL-I tests, the inter-marker distance standard deviations averaged 0.064 mm (range 0.053 to 0.085 mm; Table 2, column *a*), and the standard deviations of the included angles averaged 0.31° (range 0.20 to 0.48°; Table 2, column *c*). ACL-D test results were similar (Table 2, columns *b* and *d*).

Table 3 Anatomical Marker Placement Repeatability

	Anatomical Marker Placement Standard Deviation (mm)		
	Medial Femoral Condyle	Lateral Femoral Condyle	Femoral Head
dog 1	0.32	0.20	0.25
dog 2	0.33	0.33	0.40
doe 3	0.17	0.26	0.22
dog 4	0.33	0.34	0.07
dog 5	0.48	0.27	0.79
Average	**0.33 mm**	**0.28 mm**	**0.35 mm**

The standard deviations in anatomical marker placement (Table 3) averaged 0.33 mm for the medial femoral condyle, 0.28 mm for the lateral femoral condyle and 0.35 mm for the center of the head of the femur.

Across-trial standard deviations for tibio-femoral translations (calculated from estimated ACL origin to insertion, as described above) were similar for all three motion directions, averaging 0.14 mm (range 0.08 to 0.20 mm; Table 4 and Fig. 5). Variability in tibio-femoral rotations was more dependent on rotation axis, with across-trial standard deviations averaging 1.71° for flexion/extension, 0.90° for internal/external rotation, and 0.40° for varus/valgus rotation. For all dogs, the axis with the largest variability was also the one with the greatest range of motion during the recorded movement (flexion/extension; approximately 50° range of motion), and the axis with the smallest variability also had the smallest range of motion (varus/valgus rotation; approximately 7°; Fig. 6).

The greatest change after ACL loss was increased anterior tibial translation (Fig. 5a), as would be expected. However, ACL loss led to visible differences in all six degrees of freedom. 3D reconstructions of joint positions (100 ms after paw-strike from both ACL-intact and ACL-deficient data for the same dog) clearly show the anterior tibial shift (Fig. 7).

Estimated ligament length was nearly constant for the ACL intact trials (Fig. 8, dashed lines; mean 16.9±0.26 mm, range 16.2 to 17.4 mm). Estimated ACL origin to insertion distance increased in the ACL-D condition and showed a consistent pattern over trials. Similar results were observed in the remaining dogs.

Discussion

A method for accurate assessment of dynamic, *in-vivo* 3D bone and joint motion has been presented. The method is based on established principles and methods, including radiostereometric analysis (RSA), rigid-body kinematics and CT-based anatomical modeling. These techniques have been adapted for use with a

Table 4 Kinematic Measure Repeatability

	Across-Trial Standard Deviations: Tibio-Femoral Displacements (mm)			Across-Trial Standard Deviations: Tibio-Femoral Rotations (deg)		
	Ant-Post	Med-Lat	Prox-Dist	Flex-Ext	Int-Ext	Var-Val
dog 1	0.18	0.20	0.06	1.03	0.98	0.50
dog 2	0.16	0.15	0.14	1.62	1.07	0.38
dog 3	0.12	0.09	0.17	3.46	0.63	0.33
dog 4	0.13	0.08	0.08	1.14	0.61	0.24
dog 5	0.20	0.19	0.09	1.30	1.22	0.54
Average	**0.16 mm**	**0.14 mm**	**0.11 mm**	**1.71°**	**0.90°**	**0.40°**

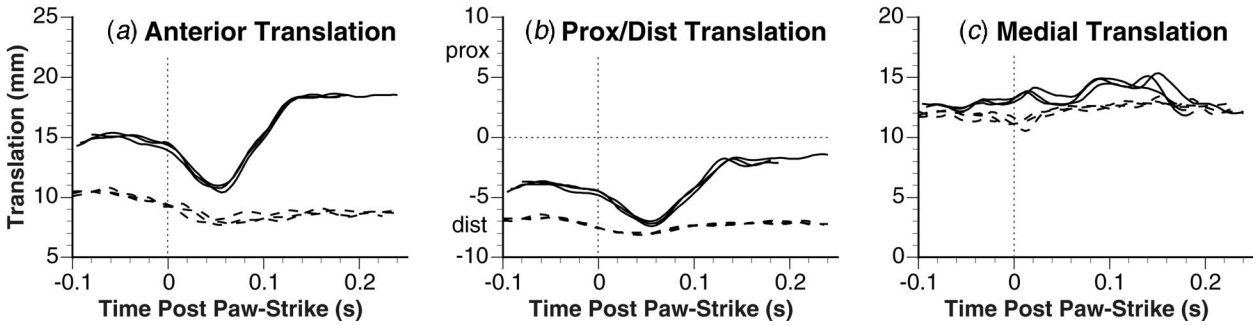

Fig. 5 Knee translation vs. time for a typical dog (Dog 1). Translations are of the tibia relative to the femur (from ACL origin to insertion), expressed in the tibial anatomical coordinate system. Three ACL-intact trials (dashed lines) and three ACL-deficient trials are superimposed. The vertical dashed line indicates pawstrike (the beginning of the stance phase). Note the dramatic increase in anterior tibial translation after ACL loss.

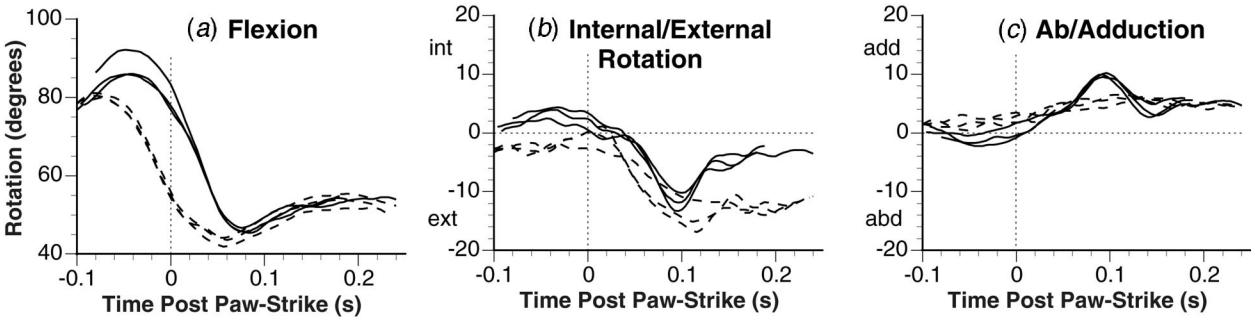

Fig. 6 Knee rotation vs. time for a typical dog (Dog 1). Rotations are of the tibia relative to the femur, expressed in the joint coordinate system as defined by Grood and Suntay [27]. Three ACL-intact trials (dashed lines) and three ACL-deficient trials are superimposed. The vertical dashed line indicates pawstrike (the beginning of the stance phase). Note that the flexion pattern differed between ACL-deficient trials, most likely due to an altered gait pattern during one of the trials.

unique high frame rate biplane radiographic imaging system, providing a powerful, precise tool for *in-vivo* dynamic joint motion measurement.

Accuracy of the system was expressed in terms of bias and precision. Dynamic bias measurements (-0.02 mm) were within the accuracy of the precision milling equipment (± 0.025 mm) used to construct the phantom object, and were not significantly different from zero. This result was predictable, as there is no physical reason to expect measurement bias in the radiographic system.

The method used to determine bias was less than ideal because the accuracy of marker placement within the test phantom was on the order of the accuracy of the system under evaluation. Thus, the difference between expected and actual distance (0.02 mm) represents an upper bound rather than an absolute measure of the system bias.

The precision of the *in-vivo* dynamic marker tracking process averaged 0.064 mm for intermarker distances and 0.31° for inscribed angles. While this level of precision may not be necessary for conventional motion studies, it is essential for studies of ligament and cartilage deformation. Furthermore, this level of accuracy is attainable on live subjects performing dynamic movements. Thus, cartilage and ligaments can be studied under truly physiological loading.

The interactive placing of anatomical markers, although relatively imprecise, has only a minor effect on kinematic measurements. The average distance between the femoral condyle anatomical markers was 21.99 mm, so a change in femoral condyle location of 0.33 mm would correspond to a change of only 0.86° in the orientation of the anatomical flexion/extension axis through the femoral condyle (anatomical y-axis). Additionally, because in practice these markers are only placed once in each bone, the location of these markers relative to the implanted tantalum markers is held constant throughout any long-term studies. Thus, small inaccuracies in their placement would produce a constant bias within a particular subject.

These estimates of accuracy are based on the assumption that all differences in inter-marker distances were the result of measurement errors. However, the two radiographic tests (ACL-I and ACL-D) were typically performed 3 months apart and the CT images were obtained 2 years after the first radiographic test.

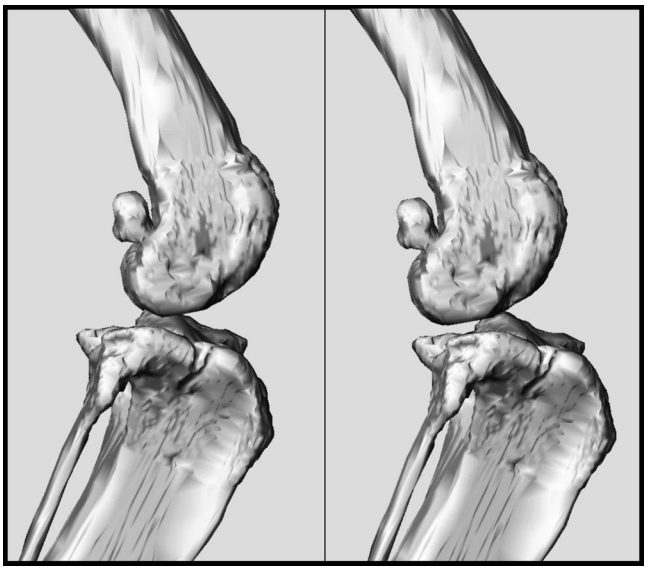

Fig. 7 3D reconstruction of tibio-femoral position for a typical dog (Dog 1). Subject-specific bone geometry was combined with kinematic data (from RSA) at 100 ms after paw-strike. After ACL loss (right image), the tibia is shifted anteriorly relative to the femur.

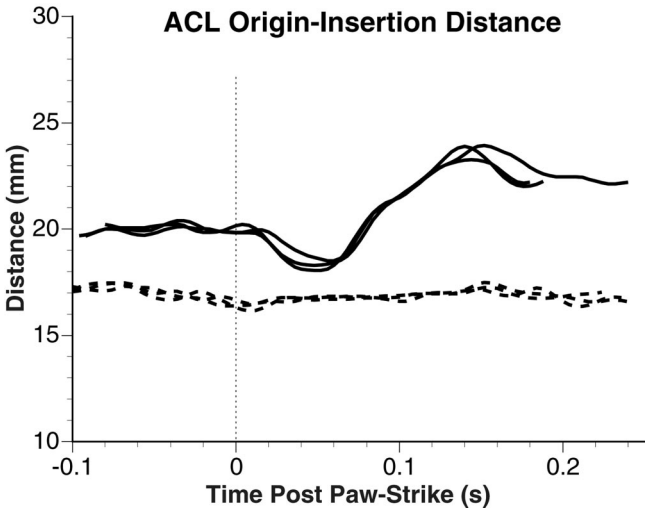

Fig. 8 ACL origin-insertion distance vs. time for a typical dog (Dog 1). The origin and insertion of the ACL were identified and marked on the 3D CT bone models. This enabled dynamic tracking of these bone locations from the marker kinematic data, and subsequent calculation of the 3D distance between these points for every motion frame. With the ACL intact (dashed lines), this distance remained nearly constant. After ACL loss, a consistent displacement between these points was observed. Three trials are superimposed for each condition.

Thus, some of these observed differences could actually have been due to migration of the markers within the bone over time or remodeling-based changes in bone geometry, though no clear evidence of marker migration was found.

Because the studies were performed *in-vivo*, it was not possible to isolate errors in the different measurement axis directions. A more controlled experiment could have been performed by *in-vitro* tracking of a bone or other object moving through a known, prescribed motion (e.g. via robotic or stepper-motor control). However, it would have been difficult to recreate aspects of the *in-vivo* tests that may contribute to measurement error, such as complex multi-axis motion, soft tissue effects, varying movement speed, etc. Because the placement of the implanted markers was somewhat random, it is likely that the combination of marker configurations spanned the major axis directions reasonably well. Within any bone, no large differences were seen in error magnitude for the different inter-marker distances. This suggests a relative independence of error from measurement direction, as would be expected from a stereophotogrammetric system with a large camera-camera angle (60° in this case).

Angular errors were reported based on actual, implanted marker configurations. These errors are very dependent on the specific geometry of the markers implanted into each bone. Markers placed closely together and/or with very small inter-marker angles can adversely affect rotational accuracy, as is the case with any marker-based rigid body tracking. For example, the markers were most poorly distributed in the femur of dog 3, with inter-marker angles of 16, 61 and 103° (all 60° angles would be ideal). This nearly linear marker configuration resulted in relatively poor flexion/extension repeatability for this dog (Table 3). However, because less than ideal marker positioning may occur during *in-vivo* studies, it is reasonable to include this animal in the reported data. It should be noted that the sizes of the canine tibias and femurs used for this study are approximately one half the size of the corresponding adult human bones. Thus, greater inter-marker spacing would be expected for human studies, which could improve rotational measurement accuracy.

As the method described is clearly invasive, it is not presented as a general replacement for conventional (video-based) motion analysis. There are risks associated with both the marker implantation and the exposure to ionizing radiation required. However, the biocompatibility of tantalum implants has been confirmed [30,31], and many years of RSA studies have demonstrated neither short nor long-term adverse consequences associated with tantalum marker implantation [19]. Additionally, the radiation (entrance) exposure for the tests described above was in the range of 200–300 mR per trial, directed only at the lower extremity. This is not considered to be high by diagnostic radiology standards (a typical knee CT study is in the range of 3000 to 4000 mR), and our Institutional Review Board has approved multi-trial human studies. These risks, though low, would support continued use of video-based motion analysis techniques (perhaps enhanced by artifact reduction algorithms) for the majority of clinical and research applications where sub-millimeter accuracy may be of little benefit.

One limitation of the technique is the need for CT data from proximal joints (such as the femoral head) near internal organs in order to construct anatomical coordinate systems. However, it may be possible to overcome this limitation by mathematically modeling the location of proximal joint centers if distal joint geometry is well defined.

This method is an attractive alternative to previously described techniques for *in-vivo* joint motion studies whenever the benefits of very high accuracy outweigh the minimal associated risks. This would likely include studies combining experimental kinematics with musculoskeletal models to estimate loads and strains in joint tissues. Since the bone geometry (from CT) is registered with the marker/bone movement, it is possible to identify and track any location on the bone surface. For example, by identifying origin and insertion points, length changes in soft tissue structures can be estimated to a high degree of accuracy. Thus, this approach is particularly well suited for the development, validation and implementation of dynamic musculoskeletal models for estimating *in-vivo* behavior of internal joint structures. This method is also well suited for studies involving rapid acceleration or deceleration, where surface marker techniques are particularly prone to skin movement error. Such motions may be critically important to investigate, since damage to biological tissues is rate-dependant and rapid changes in movement direction are often implicated in athletic injury.

References

[1] Markolf, K. L., William, B. L., Shoemaker, S. C., and Amstutz, H. C., 1981, ''The Role of Joint Load in Knee Stability,'' J. Bone Jt. Surg., **63**, pp. 570–585.

[2] Schipplein, O. D., and Andriacchi, T. P., 1991, ''Interaction Between Active and Passive Knee Stabilizers During Level Walking,'' J. Orthop. Res., **9**, pp. 113–119.

[3] Holden, J. P., Orsini, J. A., Siegel, K. L., Kepple, T. M., Gerber, L. H., and Stanhope, S. J., 1997, ''Surface Movement Errors in Shank Kinematics and Knee Kinetics During Gait,'' Gait & Posture, **5**, pp. 217–227.

[4] Reinschmidt, C., van den Bogert, A. J., Nigg, B. M., Lundberg, A., and Murphy, N., 1997, ''Effect of Skin Movement on the Analysis of Skeletal Knee Joint Motion During Running,'' J. Biomech., **30**, pp. 729–732.

[5] Lafortune, M. A., Lambert, C. E., and Lake, M. J., 1992, ''Skin Marker Displacement at the Knee Joint. NACOB II: The Second North American Congress on Biomechanics,'' Chicago, IL: Pergamon Press, J. Biomech., **26**, pp. 299.

[6] Cappozzo, A., Canati, F., Leardini, A., Benedetti, M. G., and Della Croce, U., 1996, ''Position and Orientation in Space of Bones During Movement: Experimental Artifacts,'' Clin. Biomech. (Los Angel. Calif.), **11**, pp. 90–100.

[7] Spoor, C. W., and Veldpaus, F. E., 1980, ''Rigid Body Motion Calculated from Spacial Coordinates of Markers,'' J. Biomech., **13**, pp. 391–393.

[8] Andriacchi, T. P., Alexander, E. J., Toney, M. K., Dyrby, C. O., and Sum, J., 1998, ''A Point Cluster Method for In Vivo Motion Analysis: Applied to a Study of Knee Kinematics,'' J. Biomech. Eng., **120**, pp. 743–749.

[9] Cappozzo, A., Capello, A., Della Croce, U., and Pensalfini, F., 1997, ''Surface Marker Cluster Design Criterial for 3-D Bone Movement Reconstruction,'' IEEE Trans. Biomed. Eng., **44**, pp. 1165–1174.

[10] Alexander, E. J., and Andriacchi, T. P., 2001, ''Correcting for Deformation in Skin-Based Marker Systems,'' J. Biomech., **34**, pp. 355–362.

[11] Fleming, B., Beynnon, B., Renstrom, P., Johnson, R., Nichols, C., Peura, G., and Uh, B., 1999, ''The Strain Behavior of the Anterior Cruciate Ligament During Stair Climbing: An In Vivo Study,'' Arthroscopy, **15**, pp. 185–191.

[12] Shepherd, D. E., and Seedhom, B. B., 1999, ''Thickness of Human Articular Cartilage in Joints of the Lower Limb,'' Ann. Rheum. Dis. **58**, pp. 27–34.

[13] Lafortune, M. A., Cavanagh, P. R., Sommer, H. J., and Kalenak, A., 1992, ''Three-dimensional Kinematics of the Human Knee During Walking,'' J. Biomech., **25**, pp. 347–357.

[14] Neptune, R. R., and Hull, M. L., 1995, ''Accuracy Assessment of Methods for Determining Hip Movement in Seated Cycling,'' J. Biomech., **28**, pp. 423–437.

[15] Sheehan, F. T., Zajac, F. E., and Drace, J. E., 1998, ''Using Cine Phase Contrast Magnetic Resonance Imaging to Non-Invasively Study In Vivo Knee Dynamics,'' J. Biomech., **31**, pp. 21–26.

[16] Rhoad, R. C., Klimkiewicz, J. J., Williams, G. R., Kesmodel, S. B., Udupa, J. K., Kneeland, J. B., and Iannotti, J. P., 1998, ''A New In Vivo Technique for Three-Dimensional Shoulder Kinematics Analysis,'' Skeletal Radiol., **27**, pp. 92–97.

[17] Karrholm, J., Selvik, G., Elmqvist, L.-G., Hansson, L. I., and Jonsson, H., 1988, ''Three-Dimensional Instability of the Anterior Cruciate Deficient Knee,'' J. Bone Jt. Surg., **70-B**, pp. 777–783.

[18] Selvik, G., 1990, ''Roentgen Stereophotogrammetric Analysis,'' Acta Radiol., **31**, pp. 113–126.

[19] Karrholm, J., 1989, ''Roentgen Stereophotogrammetry. Review of Orthopedic Applications.,'' Acta Orthop. Scand. **60**, pp. 491–503.

[20] Reimann D. A., and Flynn M. J., 1992, ''Automated Distortion Correction of X-Ray Image Intensifier Images,'' IEEE Nuclear Science Symposium and Medical Imaging Conference, Orlando, FL: IEEE, pp. 1339–1341.

[21] Woltring, H. J., 1980, ''Planar Control in Multi-Camera Calibration for 3-D Gait Studies,'' J. Biomech., **13**, pp. 39–48.

[22] Winter, D. A. *Biomechanics and Motor Control of Human Movement*. Wiley, New York, NY.

[23] Tashman S., DuPré K., Goitz H., Lock T., Kolowich P., and Flynn M., 1995, ''A Digital Radiographic System for Determining 3d Joint Kinematics During Movement,'' In: Williams KR, ed. 19th Annual Meeting of the American Society of Biomechanics. Stanford, CA: ASB Press, pp. 249–250.

[24] Fischer, K. J., Manson, T. T., Pfaeffle, H. J., Tomaino, M. M., and Woo, S. L.-Y., 2001, ''A Method for Measuring Joint Kinematics Designed for Accurate Registration of Kinematic Data to Models Constructed from CT Data,'' J. Biomech., **34**, pp. 377–383.

[25] Boissonnat J.-D., and Geiger B., 1993, ''Three Dimensional Reconstruction of Complex Shapes Based on the Delaunay Triangulation,'' In: Acharya RS, Goldgof DB, eds. Biomedical Image Processing and Biomedical Visualization: SPIE, pp. 964–975.
[26] Kane T. R., Likins P. W., and Levinson D. A., 1983, *Spacecraft Dynamics*, New York, McGraw-Hill.
[27] Grood, E. S., and Suntay, W. J., 1983, ''A Joint Coordinate System for the Clinical Description of Three-Dimensional Motions: Application to the Knee,'' J. Biomech. Eng., **105**, pp. 136–144.
[28] Korvick, D. L., and Pijanowski, G. J., 1994, ''Three-Dimensional Kinematics of the Intact and Cranial Cruciate Ligament Deficient Stifle of Dogs,'' J. Biomech., **27**, pp. 77–87.
[29] American Society for Testing and Materials, 1996, ''Standard Practice for Use of the Terms Precision and Bias in ASTM Test Methods,'' *Annual Book of ASTM Standards*, 14.02.
[30] Alberius P., 1983, ''Bone Reactions to Tantalum Markers. A Scanning Electron Microscopic Study,'' *Acta Anat (Basel)*, **115**, pp. 310–318.
[31] Glantz, P. O., Bjorlin, G., and Sundstrom, B., 1975, ''Tissue Reactions to Some Dental Implant Materials. An In Vivo Study in White Rats,'' Odontol Revy, **26**, pp. 231–238.